Materials Science and Engineering C 34 (2014) 54–61

Contents lists available at ScienceDirect

Materials Science and Engineering C

journal homepage: www.elsevier.com/locate/msec

Poly(vinyl alcohol)/cellulose nanowhiskers nanocomposite hydrogels for potential wound dressings

Jimena S. Gonzalez [a], Leandro N. Ludueña [a,*], Alejandra Ponce [b], Vera A. Alvarez [a]

[a] Composite Materials Group, Research Institute of Material Science and Technology (INTEMA) (CONICET-UNMdP), Solís 7575, B7608FLC Mar del Plata, Argentina
[b] GIIA Group, Research Institute of Material Science and Technology (INTEMA) (CONICET-UNMdP), Juan B. Justo 4302, B7608FDQ Mar del Plata, Argentina

ARTICLE INFO

Article history:
Received 2 June 2013
Received in revised form 27 August 2013
Accepted 10 October 2013
Available online 18 October 2013

Keywords:
Polymer-matrix composites
Nano-composites
Nano-particles
Composite hydrogel
Cellulose nanowhiskers

ABSTRACT

Polyvinyl alcohol (PVA)/cellulose nanowhisker (CNW) nanocomposite hydrogels to be used for wound dressing were obtained by freezing–thawing technique and characterized by means of morphological, physical, thermal, mechanical, barrier and antimicrobial properties. First, cellulose nanowhiskers were obtained by the acid hydrolysis of commercial crystalline microcellulose (MCC) and characterized by its size, shape, morphological, structural and thermal properties. Then, PVA/CNW nanocomposites with several CNW contents (0, 1, 3, 5 and 7 wt.%) were obtained. Morphological, thermal, chemical and physical characterization of the PVA/CNW nanocomposite hydrogels was carried out. It was found that the addition of CNW to the hydrogel allows controlling the pore morphology of the samples. On the other hand, the transparency of the samples was maintained, the thermal stability was increased, the mechanical properties were improved and the water vapor transmission rate was in the range of wound dressing applications after CNW incorporation inside the PVA hydrogel matrix. The evaluation of microbial penetration showed that the prepared hydrogels can be considered as a good barrier against different microorganisms. All obtained results indicate that the PVA/CNW materials are promising to be used as wound dressing.

1. Introduction

Substantial efforts are being lately expended to develop new materials for protecting the damaged skin from infections and dehydration [1]. The development of a new generation of wound dressings with improved healing attributes that provide an antimicrobial effect has been encouraged [1,2]. These dressings still require to be frequently changed, which may be painful to the patient, harm the vulnerable underlying skin and increase the risk of secondary contamination.

An ideal dressing should meet some requirements: creating and remaining a moisture environment, being biocompatible, absorbing fluids and exudes effectively, showing higher gas permeation, exhibiting high elasticity and also adequate mechanical strength, being transparent, and acting as a barrier against the bacterials, ensuring a protection of wound from infection and dehydration [1,3].

Hydrogel is seen as an essential component in many different types of wound care. This is because these kinds of dressings are designed to hold moisture in the surface of the wound, providing the ideal environment for cleaning the wound, absorbing the exudates and promoting the healing process [4]. The moisture in the wound is also essential in pain management for the patient, and hydrogels are very soothing and cooling.

Poly(vinyl alcohol) (PVA) hydrogels are biocompatible, non-toxic and they can absorb a huge amount of exudates [5]. Hydrogels consist in a hydrophilic polymer that forms a three-dimensional network, which swells and retains a lot of water (or biological fluids) without being dissolved. They can be obtained based on natural or synthetic polymers. Synthetic hydrogels, that have over 50% water, are notoriously brittle and have poor microstructural and mechanical stabilities [6]. For all these features PVA hydrogels can be as the right option for dressing applications. However they lack in mechanical properties.

Composites have been introduced to improve mechanical stiffness and durability [7]. The composites can be designed to meet the mechanical and physiological requirements of target application by controlling the volume fraction, morphology and physico-chemical characteristics of the reinforcement [8]. This is due to the fact that these features are responsible for the interface interaction between the polymer and the filler; the aspect ratio of the filler [9] and the dispersion of them inside the matrix [10].

Over the past decade, composite materials have attracted a great deal of interest and particular attention has been focused on the use of cellulosic fibers as reinforcements in polymer matrices for biomedical applications [11] due to their good biocompatibility [12]. The hydrolysis of cellulosic materials with a strong acid (sulfuric or hydrochloric acid) yields highly crystalline, well-defined, slender rod-like nanoparticles called cellulose nanowhiskers (CNWs) [13]. These can be about 5–10 nm in diameter and range from 100 nm to several micrometers in length depending on the origin of the cellulose (such as wood, cotton,

* Corresponding author. Tel.: +54 223 4816600x321.
E-mail address: luduena@fi.mdp.edu.ar (L.N. Ludueña).

0928-4931/$ – see front matter © 2013 Elsevier B.V. All rights reserved.
http://dx.doi.org/10.1016/j.msec.2013.10.006

bacteria, among others). The CNW shows elastic modulus as high as 130–150 GPa and strengths of 10 GPa along the axial direction [14].

Therefore, PVA/CNW nanocomposite hydrogels are ideal for different applications such as water treatments [15], soft tissue replacement [16] and drug delivery [17].

The aim of this work was to improve specific properties of PVA hydrogels as required for their use as dressings. For this purpose, composite hydrogels based on PVA and different concentrations of cellulose nanowhiskers were synthesized and characterized by means of thermal and swelling analysis, scanning electron microscopy, X-ray diffraction, mechanical and water vapor permeation measurements. Herein it was developed a reliable and a facile way to obtain nanocomposite hydrogels based on PVA with reasonable mechanical properties and excellent swelling behavior.

2. Experimental part

2.1. Materials

The PVA used in this study was a commercial product purchased from Sigma-Aldrich (USA) (Mw: of 89000–98000 g/mol, hydrolysis degree of 98–99%). The microcrystalline cellulose (MCC) was purchased from Aldrich (USA). Sulfuric acid with analytical grade was supplied by laboratory Cicarelli (Argentina).

2.2. Cellulose nanowhisker (CNW) production

CNW was prepared by the acid hydrolysis of MCC. The acid hydrolysis was carried out with sulfuric acid (H_2SO_4) solution 60 wt.% at 45 °C for 30 min under continuous stirring [15]. That solution was dialyzed for 5 days and then was spray dried in a BUCHI Mini-Spray Dryer B-290 at 185 °C.

2.3. Preparation of nanocomposite hydrogels

Aqueous solutions of 10 wt.% PVA were prepared by dissolving the polymer in distilled water at 85 °C and slowly stirring (with magnetic stirrer) for 1 h. After stirring, 1, 3, 5 and 7 wt.% of CNW (1CNW, 3CNW, 5CNW and 7CNW) were added and the stirring continued for 3 h more in order to completely dissolve the polymer. After this step, the solutions were placed in an ultrasonic bath for 30 min to remove all bubbles. The solutions were allowed to reach room temperature. Then, the PVA-based solutions were cast onto anti-adherent containers and frozen for 1 h, cooling down to −18 °C and afterward placed at room temperature (25 °C, thawing process) for the same time in order to crosslink the polymer. This procedure was repeated 3 times. To obtain the neat PVA hydrogel (PVA) the same steps were followed but without the addition of filler.

2.4. Methods

2.4.1. Characterization methods

2.4.1.1. Fourier transformed infrared (FTIR) spectroscopy. FTIR spectra of MCC and CNW were obtained in transmission mode. Samples were ground with KBr, pressed and then analyzed in a Thermo-Scientific Nicolet 6700 spectrometer, with a resolution of 4 cm^{-1}. 32 scans were performed over each sample from 600 to 4000 cm^{-1}. In the case of hydrogels, the ATR (Attenuated Total Reflectance) accessory was utilized to perform the measurements.

2.4.1.2. Thermogravimetric analysis (TGA). Dynamic thermogravimetric measurements of MCC and CNW were performed by using a Shimadzu TGA-50 instrument. Tests were run from 20 to 900 °C at a heating rate of 10 °C/min under N_2 atmosphere. In the case of hydrogels, the samples were dried (37 °C, 48 h) before test.

2.4.1.3. X-ray diffraction (XRD). Analytical Expert Instrument equipped with an X-ray generator ($\lambda = 0.154$ nm) was used to characterize the crystalline structure of the composites, fillers and matrix. Samples were scanned in 2θ ranges varying from 2 to 50° (2°/min).

2.4.1.4. Field emission scanning electron microscopy (FESEM). The morphology of MCC and nanocomposite hydrogels was analyzed by FESEM micrographs with a FE-SEM Zeiss Supra. Microcrystalline cellulose was dispersed in water, ultrasonicated and then casted in a glass, then the water was evaporated, this glass covered by MCC was coated by gold. Nanocomposite hydrogel samples were swollen, frozen, lyophilized and then cryofractured with liquid N_2 and coated by gold before testing.

2.4.1.5. Atomic force microscopy (AFM). The morphology of CNW was observed by AFM in a 5500 Scanning Probe Microscopy from Agilent Technologies operating in the contact mode in air. Samples were prepared by dispersing 5 mg of CNW in 250 mL of bidistilled water in an ultrasonic bath at room temperature for 30 min. A droplet of the resulting solution was cast onto an AFM mica disk from TED PELLA and dried in vacuum oven at 70 °C for 1 h. The resulting dispersed CNW was exposed to the AFM so as to collect contact mode images.

2.4.1.6. Differential scanning calorimetry (DSC). DSC measurements were carried out in a TA Instrument Q2000. Samples were scanned from room temperature to 250 °C at a heating rate of 10 °C/min, under N_2 atmosphere. Before DSC analysis, the hydrogel samples were dried for 24 h at 37 °C. The degree of crystallinity (X_{cr}%) was calculated from the following equation:

$$X_{cr}\% = \frac{\Delta H}{w_{PVA} \times \Delta H_c} \times 100 \quad (1)$$

where ΔH was determined by integrating the area under the melting peak over the range 190–240 °C, w_{PVA} was the PVA weight fraction and ΔHc was the heat required for melting a 100% crystalline PVA sample, 138.6 J/g [18].

2.4.2. Swelling and permeation studies

2.4.2.1. Gel fraction determinations. To perform gel fraction (*GF%*) measurements, a slice of each sample was placed in oven at 37 °C until constant weight was reached. Each sample was immersed into distilled water at room temperature for 4 days to rinse away un-reacted species. Subsequently, the immersed sample was removed from distilled water and dried at 37 °C until constant weight was reached. Therefore the gel fraction can be calculated as follows:

$$GF\% = \frac{W_f - W_F}{W_i - W_F} \times 100 \quad (2)$$

where W_i and W_f are the weights of the dried hydrogels before and after immersion, respectively, and W_F is the weight of the cellulose nanowhiskers added.

2.4.2.2. Swelling degree measurements. Swelling determinations were carried out in distilled water at 25 °C. All samples were dried before immersion at 37 °C for 48 h. The equilibrium swelling degree (M_∞ %) was determined by the following equation:

$$M_\infty\% = \frac{M_f - M_i}{M_i} \times 100 \quad (3)$$

where M_i is the weight of the samples before immersion and M_f is the weight of the sample at equilibrium water content.

2.4.2.3. Water vapor transmission rate (WVTR). For these measurements, dried hydrogel samples with a diameter of 28 ± 2 mm and a thickness

(t) of 0.16 ± 0.04 mm were cut and then put as a cap with acrylic adhesive on the mouth of a flask with a diameter of about 26 mm containing 20 mL of distilled water. The flask was then placed in a constant temperature-humidity homemade chamber for 72 h (37 °C at 75% RH). The mass loss of the system was considered as an index of *WVTR*.

The *WVTR* of each sample was calculated by using the following equation [19]:

$$WVTR\left(\frac{g}{m^2 \times h}\right) = \frac{M_0 - M_1}{72 \times A} \times 10^6 \quad (4)$$

where A is the area of flask mouth (mm^2), M_0 and M_1 are the mass of the system (flask and hydrogel cap) before and after placing it in the chamber, respectively. Because the thickness of the films varied around 25%, the *WVTR* was normalized to film thickness (t) to obtain the specific water vapor transmission rate ($NWVTR = WVTR \times t$) with units of $\left(\frac{g \times mm}{m^2 \times h}\right)$ [20].

2.4.3. Mechanical characterization: tensile tests

Tensile tests were performed in swollen state films (M_∞ %). Tests were performed in a universal testing machine Instron 3369 at room temperature and a crosshead speed of 50 mm/min. The samples were cut with rectangular shape (12 × 0.15 × 50 mm). The Young's modulus (E), stress-at break (σ_{max}) and maximum elongation-at-break (ε) were recorded.

2.4.4. Bacterial penetration assay

The bacterial penetration test was performed to evaluate the resistance of nanocomposite hydrogel wound dressings against bacterial transmission from environment to the top surface of the wound. A piece of each nanocomposite hydrogel with a diameter of 5 cm and a thickness of 3 mm was cut, then washed and sterilized several times. The sterilized sample was put on the TSA (Tryptose Soy Agar) that already incubated for 20 h at 30 °C. On the upper surface of hydrogel a suspension of bacteria (*Pseudomonas aeruginosa* ATCC 27853, *Staphylococcus aureus* ATCC 25923 and *Escherichia coli* ATCC 25922) with a concentration of 10^8 UFC/mL was dropped (10 μL), then the sample was incubated at 30–35 °C. Bacteria transport through hydrogel was monitored daily for a week via observing the growth of bacteria zone in TSA medium.

For all assay carried out in this work, the statistical method used is Student's T-test with a sample size of 3 and obtained the confidence interval for these samples.

3. Results and discussion

3.1. The filler: cellulose nanowhiskers

3.1.1. Composition and chemical characterization of MCC and CNW

The chemical composition of the MCC and CNW was analyzed by Fourier transform infrared spectroscopy. The FTIR allows characterizing the chemical structure by identifying the functional groups present in each sample.

The infrared spectra of hemicellulose, lignin and cellulose have been extensively reported in the literature [21]. The three materials are mainly composed of alkanes, esters, aromatics, ketones and alcohols, with different oxygen-containing functional groups. Changes in the chemical structure of cellulose can also be recognized by this technique.

Fig. 1 shows the FTIR spectra for the MCC and CNW. The wavelengths for the vibration of the characteristic functional groups of cellulose are clearly identified with an arrow in the spectra.

The peak in between 3060 and 3640 cm^{-1}, which was observed in both MCC and CNW spectra, is representative of the C–H and OH groups. The band at 1635 cm^{-1} is attributed to the OH bending of absorbed water. The position and the intensity of these bands were

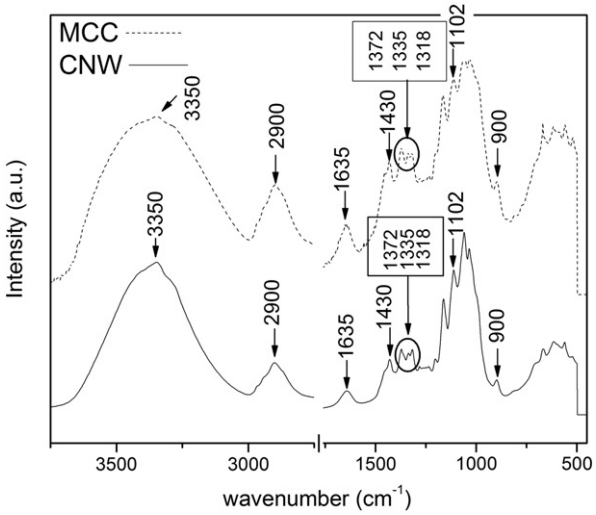

Fig. 1. FTIR spectra of MCC and CNW.

not changed indicating that the cellulose component was not removed nor degraded after the acid hydrolysis [22]. The absence of bands at 2850 cm^{-1} (C–H stretching in lignin and waxes [23,24]), 1732 cm^{-1} (vibrations of acetyl and uronic ester groups of hemicelluloses or ester linkage of carboxylic group of the ferulic and p-coumaric acids of lignin [25]), 1594–1509 cm^{-1} (aromatic ring vibrations, lignin [23,24,26]), 1460 cm^{-1} (C–H deformations, lignin [23,24]), 1235 cm^{-1} (guaiacyl ring breathing with stretching C=O, lignin [23,24]) and 1043 cm^{-1} (C–O–C stretching related with xylans associated with hemicelluloses [27]) in both MCC and CNW spectra demonstrates the high purity of both MCC and CNW, since they do not have residual contents of lignin, hemicellulose nor waxes. Changes in the chemical structure of cellulose can also be followed by FTIR. The peak at 1102 cm^{-1} was not significantly changed after acid hydrolysis, suggesting that cellulose I polymorph is present in both MCC and CNW. Fig. 1 shows thinner and less intense peak at 900 cm^{-1} after acid hydrolysis (CNW). Kavkler et al. [28] have shown that thinner peak at 900 cm^{-1} reflects less amorphous cellulose, which is expected since it is the role of the acid hydrolysis, while lower intensity at 900 cm^{-1} suggests the presence of cellulose I polymorph. The bands at 1430 cm^{-1}, 1372 cm^{-1}, 1335 cm^{-1} and 1318 cm^{-1} occur due to COH and HCC bending vibrations and are typical of crystalline cellulose [28]. These bands did not significantly change after acid

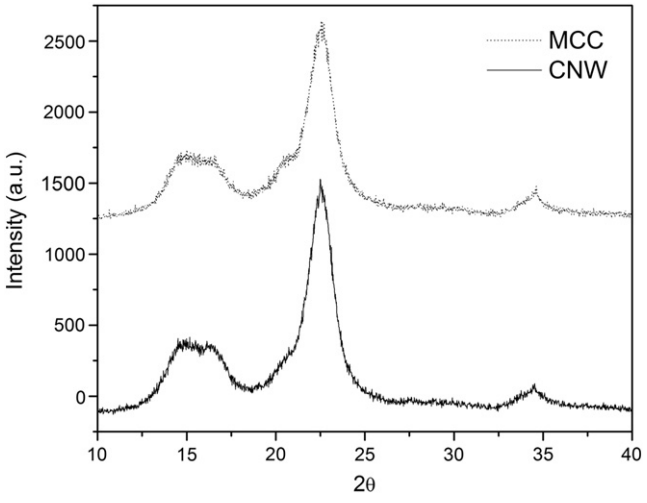

Fig. 2. XRD diffraction patterns of MCC and CNW.

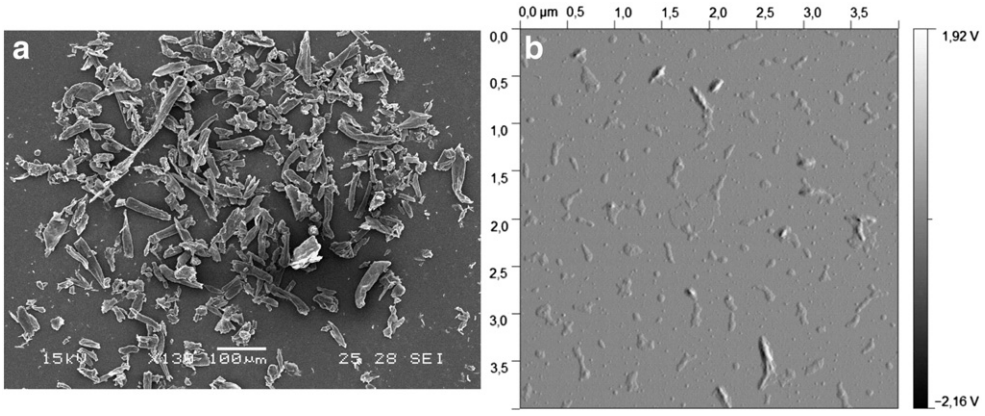

Fig. 3. Micrographs for the MCC and CNW: a) MCC, FESEM; b) CNW, AFM.

hydrolysis indicating the presence of high crystalline cellulose I in CNW [28]. The effect of acid hydrolysis removing amorphous cellulose is evident from the thinner peak at 900 cm^{-1} and less intense band at 2900 cm^{-1} in the CNW spectra [28].

3.1.1.1. Thermal stability of MCC and CNW. The thermogravimetric analysis (TGA) allows studying the thermal stability of the materials and the derivative thermogravimetric analysis (DTGA) allows identifying the temperatures at maximum weight loss rate of the components. Decomposition of both MCC and CNW showed only 2 stages. The first one corresponds to evaporation of water (small weight loss in the range 25–150 °C). It is well known that MCC and CNW are hydrophilic in nature. The moisture content (M) of MCC and CNW was calculated by the mass loss at 150 °C from the TGA curves resulting in 5.8% and 4.6% for the MCC and CNW, respectively. The values are in accordance with those reported in the literature [29]. The moisture content of MCC is higher than that of CNW which may be a consequence of amorphous cellulose removal by the acid hydrolysis [30]. The second decomposition step corresponds to cellulose thermal degradation. The maximum weight loss rate of MCC and CNW was found at 358 °C and 335 °C, respectively. In a previous work [31], we obtained similar results for CNW from cotton. Roman and Winter [32] demonstrated that the thermal degradation of cellulose crystals is catalyzed by the presence of sulfate groups which decrease the thermal stability of this component.

3.1.1.2. Crystallinity degree of MCC and CNW. The X-ray diffractometer was used to investigate the crystalline structure of the samples. The X-ray curves of the MCC and CNW are shown in Fig. 2.

The curves of both MCC and CNW showed two main peaks, one close to $2\theta = 22°$ representing the crystalline part of the materials and the other close to $2\theta = 16°$ representing the amorphous one. The presence of only one peak close to $2\theta = 22°$ suggests that crystalline cellulose is composed of cellulose I polymorph [22]. The diffraction patterns of the CNW still showed the typical reflections of cellulose I indicating that the crystal integrity had been maintained. From the obtained patterns, it is possible to estimate the crystallinity index of the materials as follows [33]:

$$I_c(\%) = \frac{\left(I_{crystalline} - I_{amorphous}\right)}{I_{crystalline}}.100 \quad (5)$$

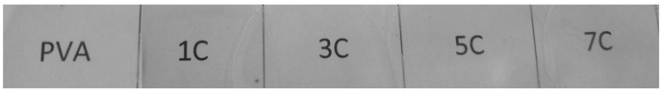

Fig. 4. Picture of PVA/CNW nanocomposite hydrogels (dried state).

where $I_{crystalline}$ is the intensity at 22° and $I_{amorphous}$ is the intensity of the peak at 2θ angle close to 16° (amorphous). The crystallinity in the MCC was 61%. In the CNW sample, a slight increase in crystallinity ($I_c = 64\%$) was observed. Similar result was obtained by Roman and Winter [32].

3.1.1.3. Morphological characterization of cellulose nanowhiskers. Fig. 3a, b shows the SEM and AFM micrographs of MCC and CNW, respectively. Length and diameter of at least 40 fibers were measured in order to make a statistical distribution. The MCC showed length (l) and diameter (d) of 71084 ± 21995 nm and 16585 ± 3072 nm, respectively, resulting in an aspect ratio (l/d) of 4.3. In the case of CNW, a reduction of almost 100% in both length (l = 158 ± 41 nm) and diameter (d = 45 ± 8 nm) was observed as a consequence of the acid hydrolysis reaction. On the other hand, the aspect ratio of CNW was slightly decreased (l/d = s3.5). The aspect ratio of CNW will be improved in future works by optimizing the acid hydrolysis conditions.

3.2. PVA/CNW nanocomposite hydrogels

3.2.1. General aspects

PVA/CNW nanocomposites were transparent for all the CNW contents (Fig. 4). This phenomenon is attributed to the nanometric size of the filler added [34].

3.2.2. Morphological, thermal, chemical and physical characterization of PVA/CNW nanocomposite hydrogels

Different mechanisms are described in the literature to explain the freezing–thawing crosslinking method. Crystallization that occurs during the freezing–thawing process is cited in the literature as the primary mechanism responsible for the resultant mechanical properties. During freezing step polymer concentrates in regions between ice crystals, promoting the generation of PVA crystals. These crystals would be responsible for gelation, acting as anchorage or crosslinking points between polymer chains. Upon thawing step and melting of ice crystals, a porous matrix would be generated by polymer-poor regions surrounded by polymer-rich gel. During consecutive freezing and thawing cycles, ice crystals would tend to preferentially create in the pores, increasing gel crystallinity density, and leading to a more resistant material [35]. Further analysis, however, shown that phase separation, independently of crystallization, was determined to have a significant effect on network forming during freeze–thaw cycling. Specially, PVA-rich regions that are formed during phase separation, without additional crosslinking, are believed to have a significant effect on the final mechanical properties [36]. Even though, other authors suggest the possibility of hydrogen bonding as the interaction responsible for the formation of the physical network [37].

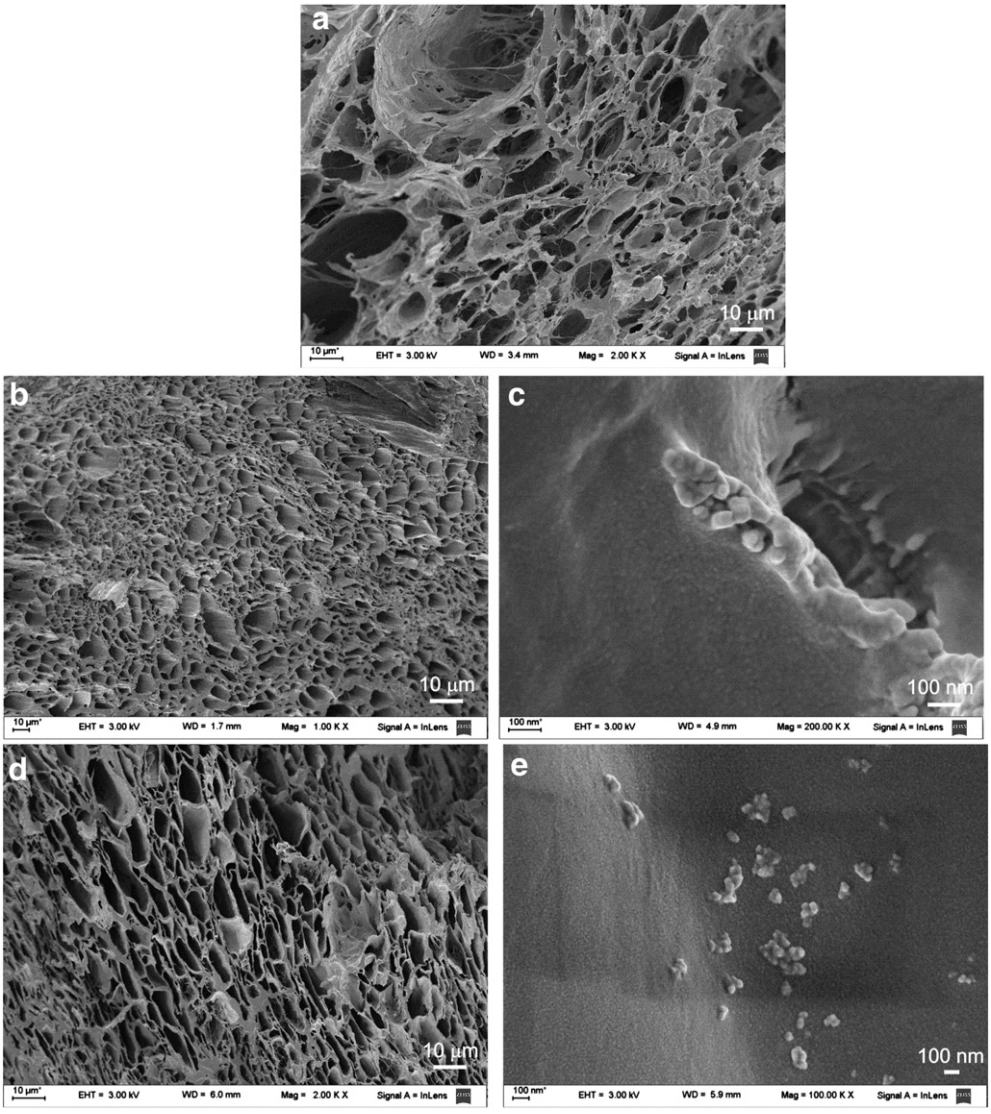

Fig. 5. FESEM images from a) PVA hydrogel, b) 1CNW c) a magnification of 1CNW, d) 3CNW and e) a magnification of 3CNW.

The highly porous structure of the hydrogels was studied by means of field emission scanning electron microscopy. FESEM images (Fig. 5) were used to analyze pore morphology and pore size distribution, as well as filler dispersion in the nanocomposite hydrogels.

The average pore diameter of PVA, 1CNW and 3CNW was 8.5 ± 4.0 µm, 6.4 ± 2.5 µm and 4.9 ± 3.6 µm, respectively. This result suggests that the filler contributes to the stability of the material. On the other hand, the pore size dispersion is more marked for the samples without reinforcement. These results indicate that the pore size can be controlled by adding cellulose nanowhiskers. Fig. 5c and e shows the magnifications of the 1CNW and 3CNW samples, respectively. Strong adhesion between CNW and PVA is expected due to the strong hydrophilic nature of both components, which promotes the formation of hydrogen bonds between the CNW and the PVA chains [38]. The formation of hydrogen bonds between the individual hydrophilic CNW fibers themselves is also favored by the great increment of their exposed surface area [13]. This phenomenon makes the CNW to have strong tendencies to agglomerate rather than disperse inside polymeric matrices. The balance between these two features of the system controls the final dispersion of the filler inside the matrix. As a consequence of this balance, Fig. 5c and e shows small CNW agglomerates of 95 ± 41 nm and 91 ± 32 nm for 1CNW and 3CNW, respectively. Taking into account that the diameter of the CNW was 45 ± 8 nm these agglomerates should be formed by no more than two or three individual CNW fibers, which can be considered as an excellent dispersion degree of the filler inside the matrix. Similar results were found for the sample 5CNW. In the case of the nanocomposite 7CNW, the material was macroscopically phase separated (not shown) and, so that, we decided to remove those samples from the study.

As it can see in Table 1, thermal and structural properties of composite hydrogels are summarized. The crystallinity degree of 1CNW is the highest one meanwhile the lowest is observed in the neat hydrogel. The rest of the composites do not show significant differences in that measurement. Results shown in Table 1 can be

Table 1
Thermal and structural properties of PVA/CNW nanocomposite hydrogels.

Sample	T_m (°C)	X_{cr} (%)	GF (%)	M_∞ (%)
PVA	228.5	48.6	83.0 ± 0.9	336.7 ± 6.4
1CNW	228.1	55.2	79.4 ± 1.9	265.2 ± 6.3
3CNW	226.6	49.2	84.8 ± 0.3	282.1 ± 6.5
5CNW	225.5	51.6	84.8 ± 4.5	263.2 ± 3.8

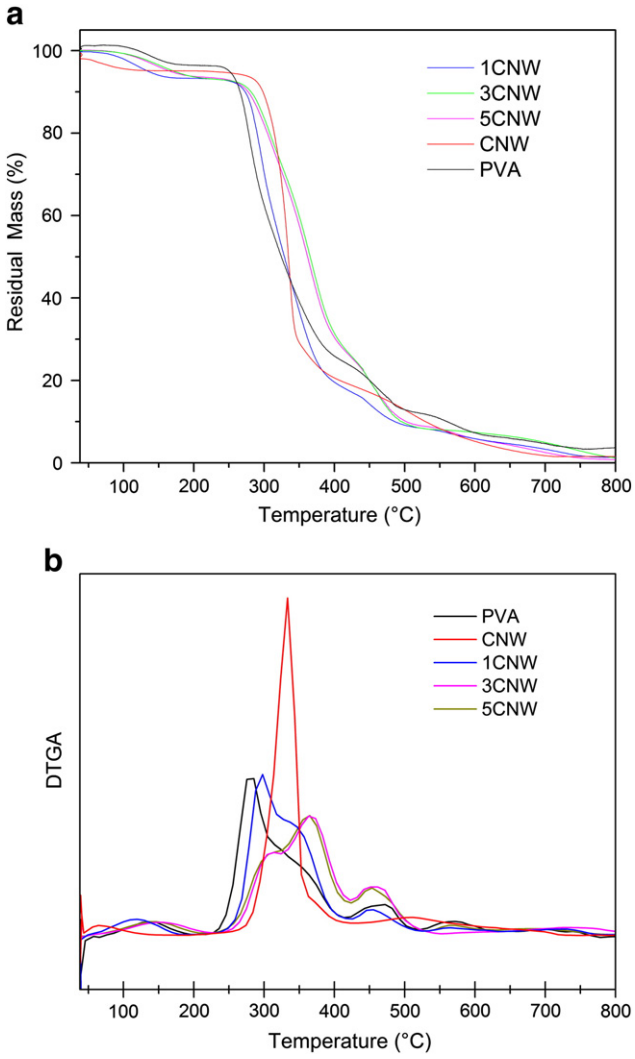

Fig. 6. Thermogravimetrical analysis of PVA, CNW and PVA/CNW nanocomposites: a) TGA, b) DTGA.

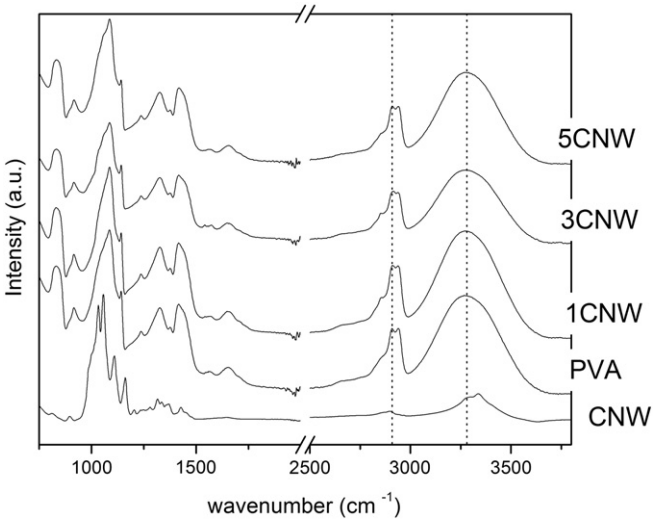

Fig. 8. FTIR spectra of neat PVA, CNW and the PVA/CNW nanocomposite hydrogels.

understood in terms of the internal organization of the PVA chains and the CNWs. It is known that the incorporation of a nano-filler can produce an increment in the nucleation sites of the polymer crystals [11], so CNWs can be acting as nucleation sites favoring the crystal formation around the nanowhiskers during the crosslinking process [11].

The *GF%* measurements do not show changes with the incorporation of CNW. This result indicates that the incorporation of CNW does not contribute to the network formation. On the other hand, the M_∞ % decreased with the addition of the filler. This behavior can be explained by the lower porous sizes of the nanocomposites in comparison with that of the neat matrix or by the interference in the water route due to the presence of the reinforcement.

The thermal degradation processes of the neat PVA, CNW and PVA/CNW studied by TGA are shown in Fig. 6. In the case of the neat PVA, five main events can be observed in the DTGA plot (Fig. 6b). The first one, located at 140 °C, corresponds to the evaporation of PVA's bound/unbound humidity. Then a peak followed by a width shoulder is observed from 220 °C to 415 °C which is related with the detachment of lateral groups forming water, acetic acid and acetaldehyde as sub-products. The main peak is associated with the thermal degradation of crystalline PVA. The shoulder is part of a peak superposed by the main one. It is related with the thermal degradation in molten state [39]. Barrera et al. [39] suggests that the detachment of lateral groups is the

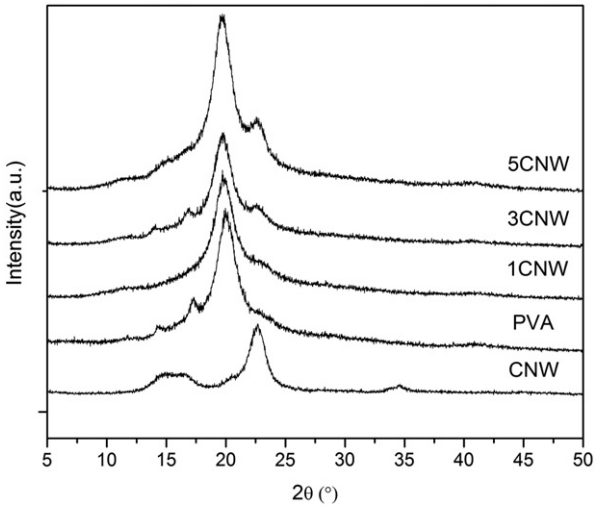

Fig. 7. XRD diffraction patterns of nanocomposites, matrix and CNW.

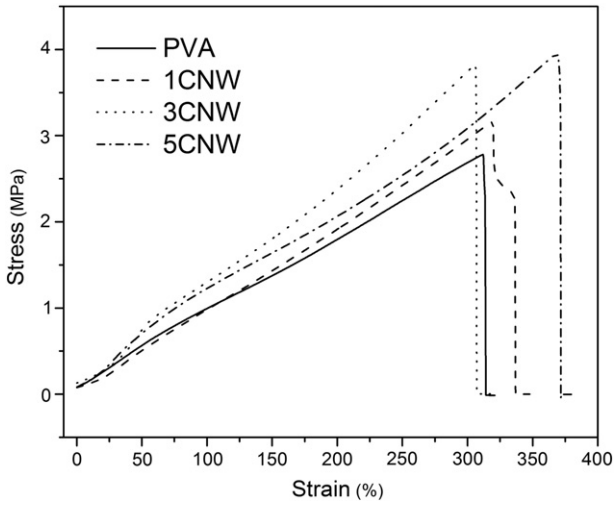

Fig. 9. Strain–stress curves from tensile tests of nanocomposites and neat matrix.

Table 2
Tensile properties and NWVTR values of neat matrix and PVA/CNW nanocomposite hydrogels.

Sample	E (MPa)	σ_{max} (MPa)	ε (%)	NWVTR ($g \cdot mm/m^2 \cdot h$)	WVTR ($g/m^2 \cdot h$)
PVA	0.8 ± 0.2	2.6 ± 1.1	294 ± 101	2.62 ± 0.29	19.7 ± 1.0
1CNW	0.7 ± 0.2	3.4 ± 0.3	369 ± 41	3.01 ± 0.27	29.9 ± 1.9
3CNW	1.1 ± 0.3	3.8 ± 0.1	343 ± 84	3.98 ± 0.36	28.4 ± 0.6
5CNW	0.9 ± 0.2	3.7 ± 0.2	336 ± 24	3.37 ± 0.36	32.9 ± 5.2

main mechanism for the thermal degradation of PVA. The peaks observed at 468 °C and 569 °C are related with the thermal degradation of the PVA main chain [39]. Fig. 6b shows that the thermal stability related with the detachment of PVA lateral groups in the nanocomposite is improved as a function of CNW content. This result indicates that the CNW acts as a thermal barrier due to the formation of hydrogen bonds between the CNW and the PVA lateral chains [38]. The thermal degradation processes related with the PVA main chain did not significantly change after CNW incorporation.

The XRD spectra of the nanocomposites, matrix and CNW are shown in Fig. 7. In the case of the nanocomposites, the peak close to $2\theta = 22°$ representing the crystalline part of the CNW can be clearly identified. The intensity of this peak is increasing as a function of the CNW content inside the nanocomposites, as was expected. The presence of only one peak close to $2\theta = 22°$ suggests that the crystalline part of CNW inside the nanocomposites is composed by cellulose I polymorph. This result indicates that the crystal integrity of CNW inside the nanocomposites has been maintained. The crystallinity index of the CNW inside the nanocomposites could not be calculated since the peak at 2θ angle close to 16° representing the amorphous part of CNW is overlapped by the peaks at 2θ angles close to 17° and 20° which are typical of neat PVA.

FTIR spectra (Fig. 8) show that adding CNW modifies the chemical structure of the gel. Compared to the neat matrix, the band of OH stretching vibration (at 3269 cm^{-1} for PVA) shifted to 3275–3280 cm^{-1} as a function of CNW amount. Moreover, the bands at 2909 cm^{-1} (C–O) were shifted to 2913–2918 cm^{-1} in the case of the nanocomposites. All these changes can be explained in terms of the interactions between the host polymer chains and the filler which alter the frequency of vibration of certain bonds.

3.2.3. Mechanical properties

Typical non-linear stress–strain response for PVA and the nanocomposites can be shown in Fig. 9. The behavior of hydrogels under the stress significantly depends on the polymer structure and the fluid inside the matrix. Once the load is applied, the polymeric chains of the hydrogel are reoriented and change their relative position; the liquid begins to drain and escape from the hydrogel. At this point it is necessary to apply a relatively small load for a significant deformation. While the application of the load continues, the orientation of the chains tends to be uniform, and the friction caused by the flow of liquid begins to produce a hardening effect of material. At this stage higher stress is required to deform the hydrogel [40].

Tensile properties of the nanocomposites reinforced with 1, 3, and 5 wt.% of CNW are summarized in Table 2. Young's modulus, stress at break and maximum elongation-at-break of all nanocomposites were improved in comparison with those of the neat matrix. It seems that the optimal concentration in terms of mechanical properties is the PVA hydrogel reinforced with 3 wt.% of CNW. These mechanical improvements can be attributed to the high CNW Young's modulus and strength. Besides, both components (filler and matrix) are hydrophilic, so the dispersion and distribution of the CNW in the PVA are benefited [41], and there is an excellent adhesion due to the several hydrogen bonds formed between them [11] as we previously showed in the morphological, chemical and physical characterization. Reinforcement effect had been observed in literature for similar systems tested by uniaxial and confined compression [42].

The values of the tensile strength of the skin are usually in the range of 2.5–16 MPa [43], and the elongation is approximately 70% in the most flexible zones [44]. It can be partially concluded that these hydrogels can be used at wound dressing in all skin zones from the most rigid to the most flexible zones.

3.2.4. Water vapor transmission rates (WVTR)

An ideal dressing would control the evaporative water loss from a wound at an ideal rate. The optimal rate should be in the mid-range of loss rates from injured skin (11 to 200 $g/m^2.h$, depending of the degree of burned) and normal skin (8.5 $g/m^2 \cdot h$) [1]. The hydrogel wound dressing must avoid or at least reduce the body liquid lost by controlling absorption and transmission as well as by maintaining the wound area wet, in order to accelerate the formation of granule and epitelesation process [45]. A higher value of WVTR causes a faster drying of the wound and a slower WVTR produces an accumulation of exudates. Table 2 also shows the WVTR and NWVTR values obtained for nanocomposite hydrogels. The NWTR value of the neat PVA increased about 15, 52 and 27% by the addition 1, 3 and 5 wt.% of CNW, respectively. Same tendency was obtained by Jipa et al. for similar systems [46]. From Table 2 it can be concluded that in all cases, WVTR values are in the optimal range for the application proposed.

3.2.5. Bacterial penetration

Daily investigation of the TSA medium showed that no bacteria were passed through the nanocomposite hydrogels during 15 days. The results indicated that only a 3 mm thickness of the nanocomposite hydrogel dressing could protect wound from bacterial penetration, while according to the previous works, it was observed that even 64 layers of gauze cannot prevent entry of exogenous bacteria into the wound. This ability of nanocomposite hydrogel dressing helps the wound from infection so that it may accelerate the wound healing [4].

4. Conclusions

Cellulose nanowhiskers (CNWs) were obtained by the acid hydrolysis of commercial crystalline microcellulose (MCC). The characterization carried out on CNW demonstrated that obtained fibers are mainly composed by cellulose with a high crystallinity index, adequate thermal stability and nanometric size.

Cellulose nanowhisker (CNW)/polyvinyl alcohol (PVA) composite hydrogels with several CNW contents (0, 1, 3, 5 and 7 wt.%) to be used for wound dressing were successfully obtained by freezing–thawing (F–T) technique.

It was found that the addition of the CNW modified the chemical structure of the gel, mainly acting as nucleation sites favoring the crystal formation around the nanowhiskers during the crosslinking process. On the other hand, it was established that the excellent compatibility between the matrix and filler (both hydrophilic) is responsible for the increment on the mechanical and barrier properties of the composite hydrogels. In addition, their function as barriers against bacterial penetration showed that they could protect the wound from further infection; hence it could accelerate the healing process of wound.

All obtained results, but mainly the mechanical, barrier and antimicrobial properties, indicate that the composite hydrogels with 03 wt.% of CNW are promising materials to be used as wound dressing.

Acknowledgments

This study was supported by the National Scientific and Technical Research Council, the National Agency of Scientific and Technology Promotion and the National University of Mar del Plata.

References

[1] F.L. Mi, S.S. Shyu, Y.B. Wu, S.T. Lee, J.Y. Shyong, R.N. Huang, Biomaterials 22 (2001) 165–173.
[2] J.J. Elsner, M. Zilberman, Acta Biomater. 5 (2009) 2872–2883.
[3] Z. Ajji, I. Othman, J.M. Rosiak, Nucl. Instrum. Methods Phys. Res., Sect. B 229 (2005) 375–380.
[4] H.J. Gwon, Y.M. Lim, S.J. An, M.H. Youn, S.H. Han, H.N. Chang, Y.C. Nho, Korean J. Chem. Eng. 26 (2009) 1686–1688.
[5] X. Li, A. Hu, L. Ye, J. Polym. Environ. 19 (2011) 398–404.
[6] Y. Tanaka, J.P. Gong, Y. Osada, Prog. Polym. Sci. (Oxford) 30 (2005) 1–9.
[7] S. Ramakrishna, J. Mayer, E. Wintermantel, K.W. Leong, Compos. Sci. Technol. 61 (2001) 1189–1224.
[8] T.W. Lin, A.A. Corvelli, C.G. Frondoza, J.C. Roberts, D.S. Hungerford, J. Biomed. Mater. Res. 36 (1997) 137–144.
[9] H. Ku, H. Wang, N. Pattarachaiyakoop, M. Trada, Compos. Part B 42 (2011) 856–873.
[10] H. Takeno, W. Nakamura, Colloid Polym. Sci. (2012) 1–7.
[11] L.E. Millon, W.K. Wan, J. Biomed. Mater. Res. B Appl. Biomat. 79 (2006) 245–253.
[12] H. Bäckdahl, G. Helenius, A. Bodin, U. Nannmark, B.R. Johansson, B. Risberg, P. Gatenholm, Biomaterials 27 (2006) 2141–2149.
[13] M.A.S. Azizi Samir, F. Alloin, A. Dufresne, Biomacromolecules 6 (2005) 612–626.
[14] T. Nishino, K. Takano, K. Nakamae, K. Saitaka, S. Itakura, J.i. Azuma, K. Okamura, J. Polym. Sci. B Polym. Phys. 33 (1995) 611–618.
[15] S.R. Shirsath, A.P. Patil, R. Patil, J.B. Naik, P.R. Gogate, S.H. Sonawane, Ultrason. Sonochem. 20 (2013) 914–923.
[16] L. Bostan, A.M. Trunfio-Sfarghiu, L. Verestiuc, M.I. Popa, F. Munteanu, J.P. Rieu, Y. Berthier, Tribol. Int. 46 (2012) 215–224.
[17] N. Sood, S. Nagpal, S. Nanda, A. Bhardwaj, A. Mehta, J. Control. Release (2013 Mar 6), http://dx.doi.org/10.1016/j.jconrel.2013.02.023 pii: S0168-3659(13)00120-X. [Epub ahead of print].
[18] S.K. Mallapragada, N.A. Peppas, J. Polym. Sci. B Polym. Phys. 34 (1996) 1339–1346.
[19] M.T. Razzak, D. Darwis, Zainuddin, Sukirno, Radiat. Phys. Chem. 62 (2001) 107–113.
[20] Y. Hu, V. Topolkaraev, A. Hiltner, E. Baer, J. Appl. Polym. Sci. 81 (2001) 1624–1633.
[21] H. Erdtman, J. Polym. Sci. B Polym. Lett. 10 (1972) 228–230.
[22] N. Johar, I. Ahmad, A. Dufresne, Ind. Crop. Prod. 37 (2012) 93–99.
[23] P. Gañán, J. Cruz, S. Garbizu, A. Arbelaiz, I. Mondragon, J. Appl. Polym. Sci. 94 (2004) 1489–1495.
[24] P. Gañán, R. Zuluaga, J.M. Velez, I. Mondragon, Macromol. Biosci. 4 (2004) 978–983.
[25] R. Zuluaga, J.L. Putaux, J. Cruz, J. Vélez, I. Mondragon, P. Gañán, Carbohydr. Polym. 76 (2009) 51–59.
[26] J.X. Sun, X.F. Sun, H. Zhao, R.C. Sun, Polym. Degrad. Stab. 84 (2004) 331–339.
[27] F. Xu, J.X. Sun, Z.C. Geng, C.F. Liu, J.L. Ren, R.C. Sun, P. Fowler, M.S. Baird, Carbohydr. Polym. 67 (2007) 56–65.
[28] K. Kavkler, N. Gunde-Cimerman, P. Zalar, A. Demšar, Polym. Degrad. Stab. 96 (2011) 574–580.
[29] N. Wang, E. Ding, R. Cheng, Polymer 48 (2007) 3486–3493.
[30] A.K. Mohanty, M. Misra, G. Hinrichsen, Macromol. Mater. Eng. 276–277 (2000) 1–24.
[31] L. Ludueña, A. Vázquez, V. Alvarez, Carbohydr. Polym. 87 (2012) 411–421.
[32] M. Roman, W.T. Winter, Biomacromolecules 5 (2004) 1671–1677.
[33] L. Segal, J.J. Creely, A.E. Martin, C.M. Conrad, Text. Res. J. 29 (1959) 786–794.
[34] S. Iwamoto, A.N. Nakagaito, H. Yano, M. Nogi, Appl. Phys. A Mater. Sci. Process. 81 (2005) 1109–1112.
[35] P.J. Willcox, D.W. Howie Jr., K. Schmidt-Rohr, D.A. Hoagland, S.P. Gido, S. Pudjijanto, L.W. Kleiner, S. Venkatraman, J. Polym. Sci. B Polym. Phys. 37 (1999) 3438–3454.
[36] J.L. Holloway, A.M. Lowman, G.R. Palmese, Soft Matter 9 (2013) 826–833.
[37] M.J. Mc Gann, C.L. Higginbotham, L.M. Geever, M.J.D. Nugent, Int. J. Pharm. 372 (2009) 154–161.
[38] L. Yang, H.Y. Zhang, Q. Yang, D.N. Lu, J. Appl. Polym. Sci. 126 (2012) E244–E250.
[39] J.E. Barrera, J.A. Rodríguez, J.E. Perilla, N.A. Algecira, Rev. Ing. E Investig. 27 (2007) 100–105.
[40] R. Ma, D. Xiong, F. Miao, J. Zhang, Y. Peng, Mater. Sci. Eng. C 29 (2009) 1979–1983.
[41] J. Wang, C. Gao, Y. Zhang, Y. Wan, Mater. Sci. Eng. C 30 (2010) 214–218.
[42] T. Abitbol, T. Johnstone, T.M. Quinn, D.G. Gray, Soft Matter 7 (2011) 2373–2379.
[43] L. Wang, E. Khor, A. Wee, L.Y. Lim, J. Biomed. Mater. Res. 63 (2002) 610–618.
[44] B. Hansen, G.B.E. Jemec, Arch. Dermatol. 138 (2002) 909–911.
[45] Huglin, M. R. (1989), Hydrogels in medicine and pharmacy Edited by N. A. Peppas, CRC Press Inc., Boca Raton, Florida, 1986 (Vol. 1), 1987 (Vols 2 and 3). Vol. 1 Fundamentals, pp. vii + 180, £72.00, ISBN 0-8493-5546-X; Vol. 2 Polymers, pp. vii + 171, £72.00, ISBN 0-8493-5547-8; Vol. 3 Properties and Applications, pp. vii + 195, £8000, ISBN 0-8493-5548-6. Brit. Poly. J., 21: 184. http://dx.doi.org/10.1002/pi.4980210223.
[46] I.M. Jipa, M. Stroescu, A. Stoica-Guzun, T. Dobre, S. Jinga, T. Zaharescu, Nucl. Instrum. Methods Phys. Res., Sect. B 278 (2012) 82–87.